

## Body-wave extraction from ambient noise recorded by a dense array

Nori Nakata (Stanford University)

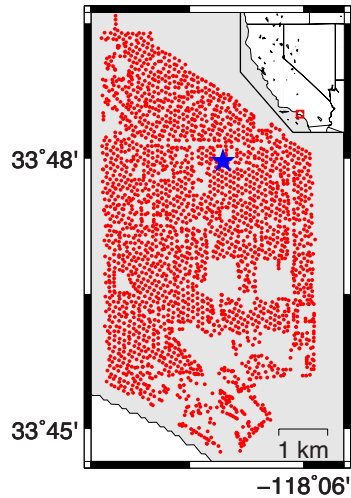


Figure 1: Map of receivers. The red dots show the location of receivers, and the blue star indicates the reference receiver used in Figure 2a. The red square in the inset shows the location of the survey.

### SUMMARY

I retrieve P diving waves by applying seismic interferometry to ambient noise records observed at Long Beach, California, and invert travel times of these waves to estimate 3D P-wave velocity structure. The ambient noise is recorded by a 2D dense and large network, which has about 2500 receivers with 100-m spacing (Figure 1). In contrast from surface-wave extraction, body-wave extraction is much harder because body-wave energy is smaller than surface waves. The crosscorrelation functions at a receiver pair obtained from ambient-noise data does not show clear body waves. Although I can reconstruct body waves when I stack correlation functions over all receiver pairs, I need to extract body waves at each receiver pair separately for imaging spatial heterogeneity of subsurface structure. Therefore, I employ two filters after correlation to seek body waves between single receiver pairs: selection of traces and noise suppression. After these steps, I can reconstruct clear body waves from each virtual source. As an application of using extracted body waves, I estimate 3D P-wave velocities from these waves with travel-time tomography. The velocities estimated from body waves are much higher resolution than those from surface waves.

### RETRIEVAL OF BODY WAVES AND TOMOGRAPHY

I use 10-day ambient-noise data recorded at all stations to retrieve body waves. Figure 2a shows an example of gathers of correlation functions with a reference station at the blue star

in Figure 1. To plot the virtual-shot gather, I sort the traces by offset between the virtual source and each receiver (not depending on azimuth). In Figure 2a, although I can reconstruct strong surface waves with apparent wave speeds between 0.4–0.9 km/s, I cannot find clear coherent signals faster than 1.5 km/s (e.g., P waves). When I use all virtual-source gathers to enhance body waves by stacking correlated waveforms over all receiver pairs in each 50-m distance bin from each virtual source. After binning stacking, I can obtain clear body waves that propagate faster than 1.5 km/s (Figure 2b; as expected from Lin et al. (2013)). Because the wave starts propagating at roughly zero time lag and the apparent velocity of the wave increases at far offsets, I assume that this reconstructed wave is a P diving wave.

For obtaining high-resolution spatial information of subsurface, I need to extract body waves from each pair of traces (i.e., from individual virtual shot gathers such as the gather in Figure 2a). I employ two steps to isolate body waves contained within the individual crosscorrelation functions. First, I select daily correlations which include relatively strong body-wave energy. For this selection, I use body waves in Figure 2b as an example. I compute a second crosscorrelation between each daily correlation in Figure 2a and a corresponding trace at a bin of the appropriate distance in Figure 2b. When these traces have a high correlation value, I keep the trace of the daily correlation. After this filter, I retain about 35% of traces that contain stronger body waves.

This second step involves an adaptive covariance filter (ACF), which is designed for ambient-noise analyses (Lawrence, 2014) to extract coherent energy and suppress unwanted noise from correlation functions, where I assume that real signals are coherent and noise is incoherent. When I classify retained traces at each bin and each time lag of the maximum value of second correlation, the body-wave signals of traces in each class are coherent, which means arrival times and spectra of all body waves are similar. Then I apply the ACF to traces in each class for making body waves clear enough to use tomography.

After I extract body waves from each virtual-shot gather and estimate arrival times for the waves, I have about two million travel times. With these travel times, we implement body-wave tomography based on Hole (1992), assuming diving body waves. Figure 3 shows vertical and horizontal slices of the inverted 3D P-wave velocity structure. We invert the data with several 1D starting models and update the initial models during inversion. Figures 3a–c show P velocity perturbations relative to the best-fit 1D velocity (Figure 3d). Based on the ray coverages, diving waves reach up to 1.2-km depth (the largest offset we can find body waves is 8.6 km). The errors of the velocities are around 0.5–1%, which is small enough to interpret lateral and vertical velocity heterogeneities in Figure 3. Nakata et al. (2014) show more detail of the data and filters.

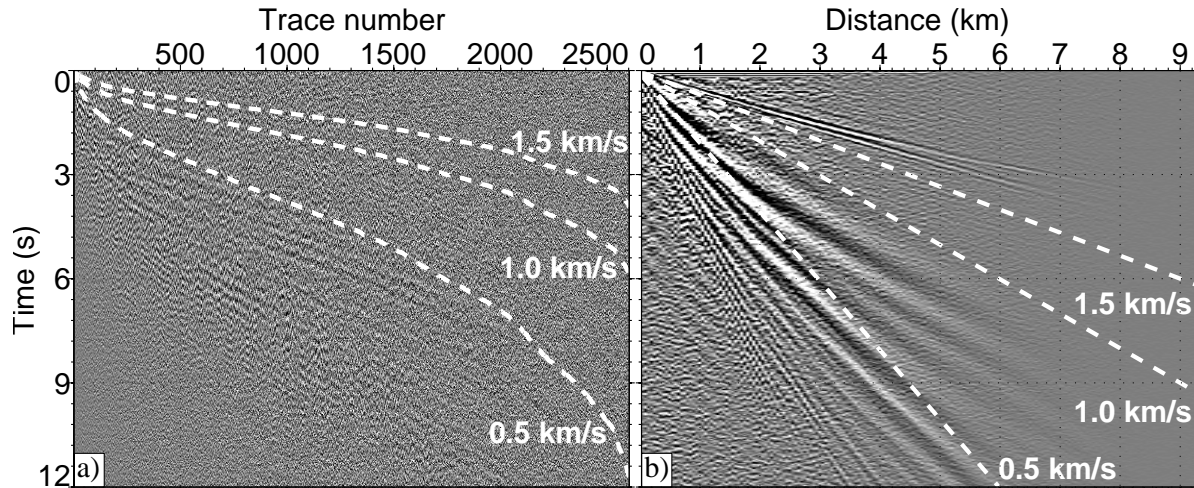


Figure 2: (a) Example of virtual shot gathers constructed from 10 days of ambient-noise data. The virtual source is at the blue star in Figure 1. Trace numbers are sorted by the distance from the virtual source. The frequency range is from 0.5 to 15.0 Hz. (b) Stacked crosscorrelation gather over all virtual shot gathers according to offsets of receiver pairs. The size of each bin for this spatial stacking is 50 m. The frequency range is the same as panel (a). The white lines in all panels indicate travel times with constant velocities with an assumption of straight ray paths.

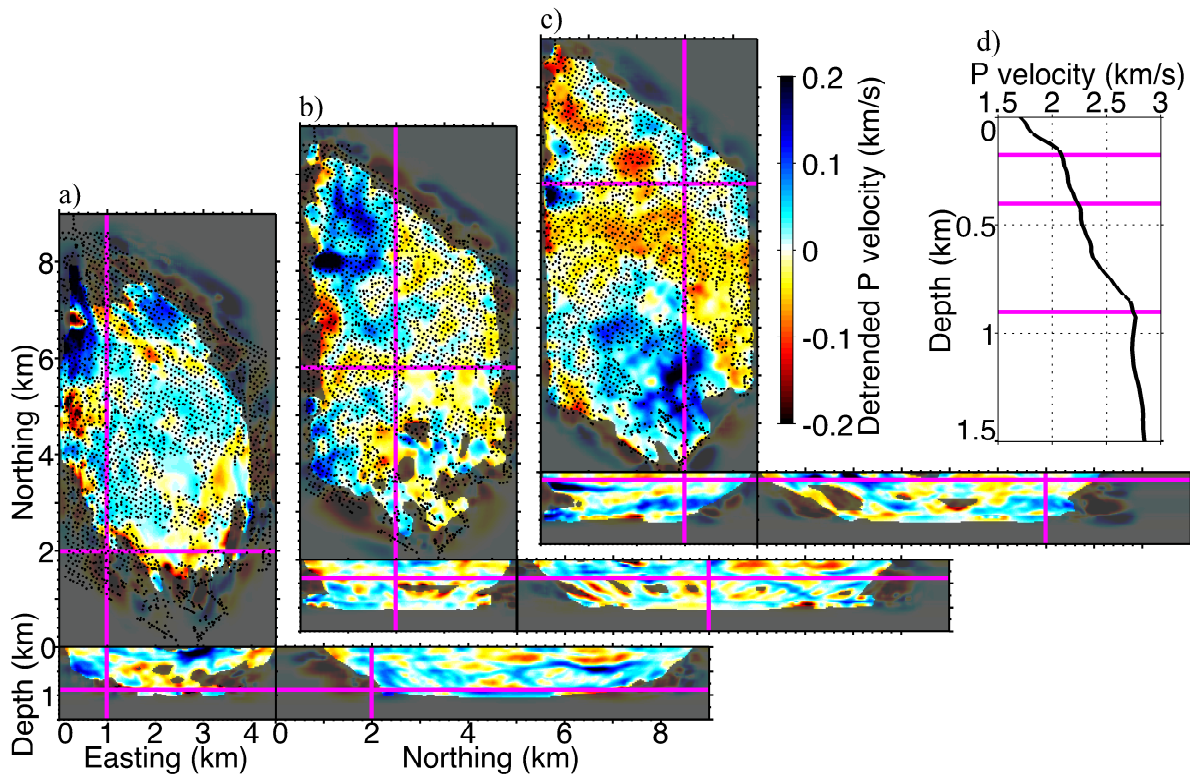


Figure 3: Vertical and horizontal slices of inverted P-wave velocity cube. From (a)–(c), slices shift shallower, east, and north. The magenta lines show the location of slices, and the depths of horizontal slices are 0.17, 0.40, and 0.90 km. Velocities are detrended by subtracting the horizontally averaged 1D velocities shown in panel (d). The colormap is valid for panels (a)–(c), where blue indicates velocities faster than the velocity at the corresponding depth in panel (d). The shaded areas in the velocity slices are poor ray coverage areas. The origin of the local coordinate in this figure (Easting = 0 km and Northing = 0 km) is the southwest corner in Figure 1.

## REFERENCES

- Hole, J. A., 1992, Nonlinear high-resolution three-dimensional seismic travel time tomography: *J. Geophys. Res.*, **97**, 6553–6562.
- Lawrence, J. F., 2014, Improved seismic ambient noise analyses with the adaptive covariance filter: *J. Geophys. Res.*(in review).
- Lin, F.-C., D. Li, R. W. Clayton, and D. Hollis, 2013, High-resolution 3D shallow crustal structure in Long Beach, California: Application of ambient noise tomography on a dense seismic array: *Geophysics*, **78**, Q45–Q56.
- Nakata, N., J. P. Chang, and J. F. Lawrence, 2014, Body-wave extraction and tomography at Long Beach, CA, with ambient-noise tomography: *J. Geophys. Res.*(submitted).

## ACKNOWLEDGMENTS

We are grateful to Signal Hill Petroleum, Inc. for access to this dataset and permission to publish. We also thank Dan Hollis, John A. Hole, Jason P. Chang, Jesse F. Lawrence and Biondo Biondi for their professional help and comments.